Annals of Biomedical Engineering, Vol. 39, No. 1, January 2011 *(© 2010)* pp. 85–95
DOI: 10.1007/s10439-010-0125-0

Application of Optimization Methodology and Specimen-Specific Finite Element Models for Investigating Material Properties of Rat Skull

FENGJIAO GUAN,[1,2] XU HAN,[1] HAOJIE MAO,[2] CHRISTINA WAGNER,[2] YENER N. YENI,[3] and KING H. YANG[1,2]

[1]State Key Laboratory of Advanced Design and Manufacturing for Vehicle Body, Hunan University, Hunan, China; [2]Bioengineering Center, Wayne State University, 818 W. Hancock, Detroit, MI 48201, USA; and [3]Henry Ford Hospital, Detroit, MI, USA

(Received 19 April 2010; accepted 5 July 2010; published online 23 July 2010)

Associate Editor Kyriacos A. Athanasiou oversaw the review of this article.

Abstract—Finite element (FE) models of rat skull bone samples were developed by reconstructing the three-dimensional geometry of microCT images and voxel-based hexahedral meshes. An optimization-based material identification method was developed to obtain the most favorable material property parameters by minimizing differences in three-point bending test responses between experimental and simulation results. An anisotropic Kriging model and sequential quadratic programming, in conjunction with Latin Hypercube Sampling (LHS), are utilized to minimize the disparity between the experimental and FE model predicted force–deflection curves. A selected number of material parameters, namely Young's modulus, yield stress, tangent modulus, and failure strain, are varied iteratively using the proposed optimization scheme until the assessment index '*F*', the objective function comparing simulation and experimental force–deflection curves through least squares, is minimized. Results show that through the application of this method, the optimized models' force–deflection curves are closely in accordance with the measured data. The average differences between the experimental and simulation data are around 0.378 N (which was 3.3% of the force peak value) and 0.227 N (which was 2.7% of the force peak value) for two different test modes, respectively. The proposed optimization methodology is a potentially useful tool to effectively help establish material parameters. This study represents a preliminary effort in the development and validation of FE models for the rat skull, which may ultimately serve to develop a more biofidelic rat head FE model.

Keywords—Rat skull, Specimen-specific finite element models, Anisotropic Kriging, Optimization, Material identification.

INTRODUCTION

Numerous *in vivo* rodent experimental models have been developed to investigate different types of traumatic brain injury (TBI), associated behavioral changes, and efficacy of therapeutic methods. Although the external parameters used in these experimental models (such as the impact speed, impact depth, and weight of the impactor) can be precisely controlled, there are no direct methods available for investigating intracranial responses that are directly related to tissue damage. At present, finite element (FE) models are probably the best means to acquire such responses. In recent years, several FE models of the rat head have been developed to predict internal responses of the brain under injury scenarios to complement experimental studies.[17–20,24] In order to ensure accurately predicted brain internal responses using FE modeling techniques, accurate material properties are necessary.

Several studies have been conducted to determine human cranial bone properties in different loading modes and directions.[21,23] In the adult, cranial bone can be divided into compact bone (outer and inner tables) and trabecular bone (diploë), which have been tested both as a composite and separately. Melvin *et al.*[23] found that the compressive modulus of the human diploë layer ranged from 0.39 to 2.75 GPa. For the intact three-layered structure, McElhaney's study of dog-bone shaped human skull samples in in-plane tension indicated an average elastic modulus of 5.38 (±2.90) GPa,[21] with no significant differences found in compressive modulus when skull bone samples were tested in different tangential directions. Testing of human skull bone perpendicular to the surface has resulted in an elastic modulus of 2.4 GPa,[21] but other studies have reported values of half that magnitude.[1,28] To the best of our knowledge, only one study has reported the material properties of rat skull bone.[8] That study utilized several two-dimensional FE models to simulate indentation tests conducted on rat skulls to

Address correspondence to King H. Yang, Bioengineering Center, Wayne State University, 818 W. Hancock, Detroit, MI 48201, USA. Electronic mail: king.yang@wayne.edu

calculate material property parameters. The authors reported an average elastic modulus of 6.01 MPa for the skull of 43-day-old adult rat, which was at least 60 times lower than that of human. Some of the difference in moduli between rat and human skulls may be due to variance in porosity or trabecular arrangement of these bones, in addition to the indirect method used by Gefen *et al.*[8] to determine the skull bone properties.

Experimentally, machining a small, curved rat skull into rectangular specimens for direct material testing may present some technical challenges. Additionally, no literature has been published to date reporting rat skull properties at different loading rates. Finally, although optimization methods have been used in biomaterial identification problems,[4,14,32,33] little information was provided regarding which optimization procedures were applied.

The primary objective of this study was, therefore, to develop a methodology for investigating rate-dependent elastic–plastic properties (Young's modulus, yield stress, tangent modulus, and failure strain) of the rat skull. Experimental three-point bending tests at two different rates were conducted to obtain force–deflection curves. Considering that each skull sample had different dimensions and varying porosities, specimen-specific FE models were developed and used in conjunction with optimization-based material identification method to match experimentally measured and model predicted force–deflection curves to identify aforementioned material property parameters.

MATERIALS AND METHODS

Geometry and Hexahedral Mesh Generation

Two skull samples, each approximately 14 by 3 mm, were dissected using a Dremel rotary tool (Model 750, Robert Bosch Tool Corporation, IL) from each of 10 young adult Sprague-Dawley rats with an average mass of 266 (±7) g. The microcomputed tomography (microCT) scanner built in-house at Henry Ford Hospital (Detroit, MI), similar to the original system previously described by Reimann *et al.*,[26] was used to scan all 20 samples at a spatial resolution of 16 × 16 × 16 μm to depict detailed geometric profiles and internal porosities. Figure 1 shows a coronal section of a typical sample with detailed geometric structure obtained from microCT scanning, in which the porous characteristics are shown. The average thickness of each skull sample was measured from the microCT images. An imaging post-processing software, Mimics (version 12, Materialise Inc., Leuven, Belgium), was used to segment the bony portion from each microCT dataset before a voxel-based hexahedral mesh was generated to create sample-specific FE meshes with an element resolution of 64 × 64 × 128 μm (Fig. 2). The sample-specific FE models served to eliminate any geometric effect due to intersample variations, such as varying thickness and locations without bony tissues (i.e., voids or holes), on model predicted force–deflection curves.

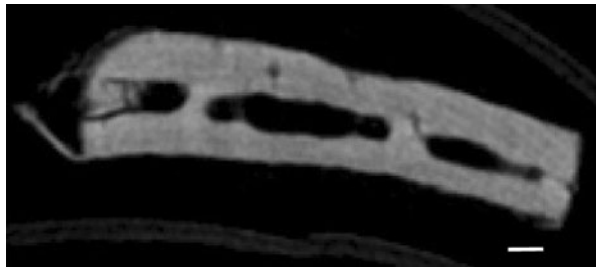

FIGURE 1. A typical microCT image showing the porosity of one skull sample. The *size bar* indicates 200 μm.

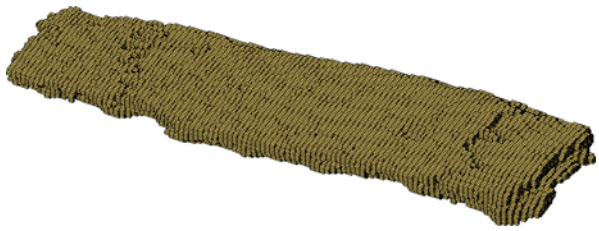

FIGURE 2. A sample-specific FE mesh of one skull sample using 35,613 hexahedral elements.

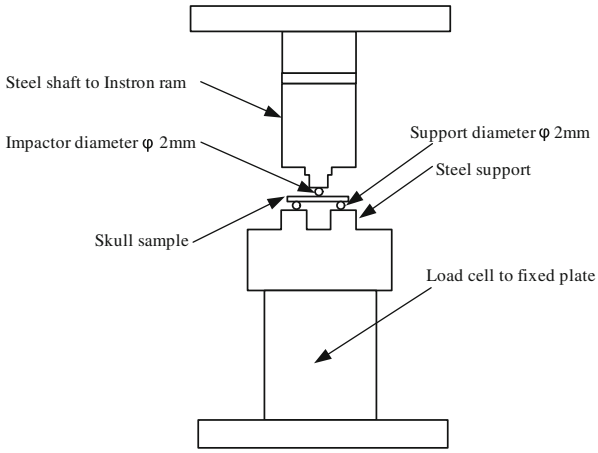

FIGURE 3. Schematic diagram of the three-point bending test setup.

Three-point Bending Test Setup

The two samples taken from each rat were tested in three-point bending on an Instron material testing system (Model 1321 frame with Model 8500 controller, Canton, MA) at a randomly selected loading velocity of either 0.02 or 200 mm/s using the test setup shown in Fig. 3. The center of loading was aligned with the

mid-point between the bregma and lambda sutures. The long axis of a cylindrical steel rod with a diameter of 2 mm served as the impactor surface, held in place by a solid steel shaft attached to the Instron ram with an aluminum plate. Two other rods of the same diameter were used to support the specimen during bending. A 22.24 N capacity load cell (Model MDB-5, Transducer Techniques, CA), screwed firmly to the Instron frame underneath the sample supports, was used to measure the force–time histories. SAE channel frequency class (CFC) 600 filter at a corner frequency of 1000 Hz was used to filter all force–time curves. Equation (1), taken from classical beam theory, was used also to calculate the Young's modulus from three-point bending test results for comparison with optimization results:

$$E = \frac{L^3 m}{4bd^3} \tag{1}$$

where E stands for the elastic modulus in MPa; L stands for support span in mm; m stands for slope of the initial straight line portion of the force–deflection curve in N/mm; b stands for width of test sample in mm; and d stands for thickness of test sample in mm.

FE Simulations

The boundary and loading conditions were precisely defined for each FE model using Hypermesh (Altair Engineering, Troy, MI) according to the specimen-specific experimental setup. The implicit FE method is generally the preferred method when solving quasi-static problems. When the entire system's degrees-of-freedom are very large, this method requires an enormous amount of random access memory to store the structural stiffness matrix before it is inversed to calculate nodal displacements. It may become very computationally expensive when acquiring time histories at small time steps as compared to using the explicit FE method. Additionally, the current optimization study called for a large number of simulations to determine optimal material parameters. Consequently, shortening the time needed for each simulation was greatly desired. One way to overcome these problems is through the application of a damping factor using the explicit solver, so long as the kinetic energy is controlled near zero. This method is recommended by the LS-DYNA theory manual and has been used successfully by Zhang.[10,36]

To simulate quasi-static loading at 0.02 mm/s with minimal computational time and random access memory, a damping factor was applied in the LS-DYNA explicit solver to ensure that the kinetic energy was close to zero. An iterative process was set up to choose the best damping factor until the kinetic energy nearly vanished. This resulted in a damping factor (ξ) of 60 ms^{-1} for one skull sample. To check its validity, the force–deflection curve predicted by the combined explicit solver with the addition of 60 ms^{-1} damping factor was then compared to that predicted using the implicit method. Figure 4 demonstrates that the differences between implicit and explicit predictions were minimal (less than 1%). Subsequently, the same damping factor was applied to all quasi-static simulations to calculate the optimal material properties. In solving high-speed transient dynamic problems using an explicit FE solver, no damping factor is needed as long as the time step is smaller than that needed for the wave to pass through each element.

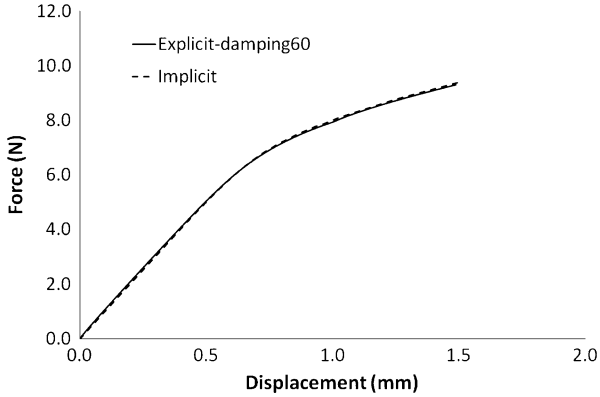

FIGURE 4. Comparison between implicit solution method and explicit solution method.

The constitutive material law assumed was *MAT_PIECEWISE_LINEAR_PLASTICITY from the LS-DYNA material library. In order to reduce the simulation time, a Massively Parallel Processing (MPP) version of the solver was used on an eight-node cluster, which has two AMD Opteron (tm) processors with a clock speed of 2.4 GHz for each node.

Optimization-based Material Identification

The objective function selected for the optimization scheme was based on an assessment index F, which aimed to minimize the average error between the experimentally obtained and model calculated force–deflection curves on a least squares basis, as shown in Eq. (2).

$$F = \sqrt{\sum_{i=1}^{n} (f_{\mathrm{m}i} - f_{\mathrm{c}i})^2 \Big/ n} \tag{2}$$

Here $f_{\mathrm{m}i}$ indicates those values measured from tests, $f_{\mathrm{c}i}$ indicates the FE model calculated corresponding force values, m stands for the "measured" value, c stands for the "calculated" value, and n stands for the number of points of measured data. Different loading speeds

require different n values, which are determined by total loading time and sampling frequency. In this study $(f_{mi} - f_{ci})^2$, in correspondence with the absolute difference, was adapted in the assessment index (Eq. 2) instead of $(f_{mi} - f_{ci})^2/f_{mi}$, related to relative difference, to avoid over-fitting of the initial phases of elastic deformation. The sampling interval in each simulation was 0.02 ms. As evident from Eq. (2), an F value of zero (0) represents the best possible match.

As in any material testing, the force–deflection curve drops sharply after failure occurs. To minimize over-exaggeration of this effect on curving fitting, the magnitude of failure strain was matched separately. Therefore, the material identification of each skull sample was divided into two stages. In the first stage, the force–deflection curves before failure were used to determine the most favorable Young's modulus, yield stress, and tangent modulus based on the optimization procedures. In the second stage, an FE analysis based on the Young's modulus, yield stress, and tangent modulus obtained in the first stage was performed to fit the time of failure with an appropriate failure strain. Thus, over-fitting of the curve based on post-failure behavior is avoided. In this manner, precise failure strain can be revealed more clearly.

A "design domain" which covered the possible range of the Young's modulus, yield stress, and tangent modulus was defined. Because the Young's modulus in the case of skull bone is loading rate-dependent,[35] the ranges of Young's moduli under the two different loading conditions could be dissimilar, with the lower loading rate resulting in a lower value of Young's modulus. The ranges selected for identifying the optimized Young's modulus, yield stress, tangent modulus, and failure strain for each specimen are listed in Tables 1 and 2. These ranges define a feasible domain of the parameters to be identified. An optimization software modeFRONTIER (Esteco, Srl, Itlay) was used to automatically update these input parameters and submit the new keyword file to LS-DYNA, which ran in MPP mode, to reduce the time needed to complete the task.

The Latin Hypercube Sampling (LHS) method (further described in "LHS Method" section) was then used to obtain a uniform allocation inside the design domain. A sequential quadratic program (further described in "Sequential Quadratic Programming Algorithm" section) was then used to find the minimal F from the response surface formed by an anisotropic Kriging model (further described in "Anisotropic Kriging" section). It is proposed that the combination of Design of Computer Experiments (DOCE), response surface method, and optimization technique is ideal for reverse engineering, taking into account a certain degree of uncertainty in the physical experiments. At the end of the optimization, the optimal material parameters obtained from this procedure are used as input to specimen-specific FE models undergoing validation. This process is desired to judge the validity of the response surface.

TABLE 1. Range of design parameters for loading velocity of 200 mm/s.

No.	Parameters	Lower bound	Upper bound
1	Young's modulus (GPa)	10.00	20.00
2	Yield stress (GPa)	0.050	0.180
3	Tangent modulus (GPa)	0.01	1.80
4	Failure strain	0.010	0.150

TABLE 2. Range of design parameters for loading velocity of 0.02 mm/s.

No.	Parameters	Lower bound	Upper bound
1	Young's modulus (GPa)	6.00	15.00
2	Yield stress (GPa)	0.050	0.180
3	Tangent modulus (GPa)	0.005	0.150
4	Failure strain	0.010	0.150

Figure 5 shows the flowchart used to identify the material property parameters of each sample using modeFRONTIER version 4.1 with the Young's modulus, yield stress, and tangent modulus as design variables and F as the objective function of the optimization study.

LHS Method

A response surface identified through an anisotropic Kriging model was proposed here to find the optimal material parameters that minimize F. Considering the large range of material properties to be investigated, there is a need to reduce the number of FE simulations before utilizing the anisotropic Kriging model. The DOCE method is aimed at minimizing the number of runs while simultaneously acquiring as much information as possible. There are several DOCE methods that have been proposed in the literature.[7,29–31] Many methods allow only two to three levels for each input variable to avoid a rapid increase in the number of computer experiments.

The LHS technique, which has been used extensively in many DOCE, was adopted in this study. LHS was first proposed by McKay *et al.*[22] and has become one of the most popular design types for Kriging models. LHS is a space-filling design with constrainedly stratified sampling method. Once the number of computer experiments (n) is determined, each input range of input variables (m) is split into n intervals of equal length and form an n^m grid on the experimental space. Independent

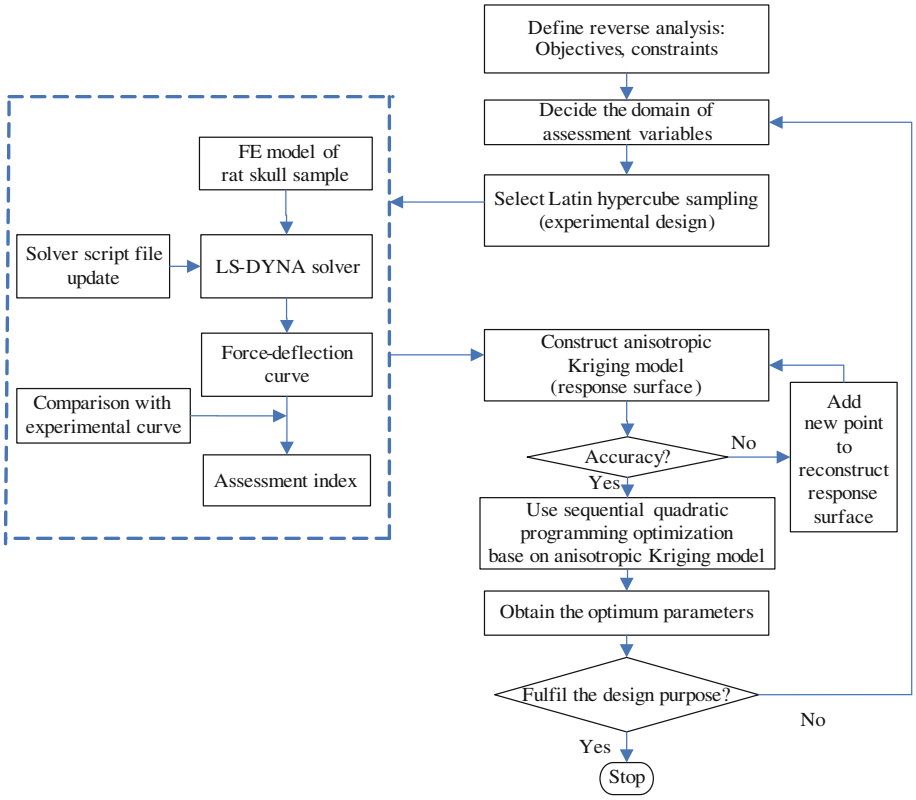

FIGURE 5. Optimization procedures used to determine material parameters.

sampling with the same probability is then performed within each subinterval. Random samples from subintervals can be taken one at a time, while this technique remembers which samples were taken so far. Thus, n points are selected among the grid so that n levels of each variable are represented only once in the design domain. In this way, the exact input values are relatively uniformly sampled over the design space. Also note that this sampling scheme does not require more samples for more variables; therefore, the key advantage of this technique is that the number of samples does not increase exponentially with the number of variables, and at the same time it ensures that a small number of computer experiments with multiple levels will be sufficient to investigate the potentially nonlinear relationships between input variables and output response. As illustrated in Fig. 6 for a two-dimensional problem, each variable in an LHS scheme is divided into five equal subintervals and then organized simultaneously to form a matrix of random sampling points to ensure that all portions of the design space are captured.

The number of simulations in LHS is determined by the total number of design variables involved. To construct a reasonably accurate approximated model for optimization, Gu and Yang[9] recommended a minimum of three times the number of design variables to be used for initial simulations. Based on this assumption, for each test sample, 12 FE model simulations were conducted initially within the design space to construct the first response surface.

Anisotropic Kriging

After generating the LHS sample points, FE simulations were completed using LS-DYNA. The corresponding assessment indices (F), calculated from these simulations, were used as the response to construct the approximated model. Some literature sources indicate that a simple polynomial model may not be sufficient for modeling complex nonlinear responses.[2,12,16,29,30] For example, second-order response surfaces are incapable of modeling surfaces with multiple extrema because they do not have a very flexible shape.

An anisotropic Kriging model was adapted here to construct the approximate model. Anisotropic Kriging is a refined version of the Kriging model which offers the possibility of controlling the relative importance between input variables.[25]

The basis of the Kriging response surface method is the estimation of the response as a combination of two components, a global model plus a localized departure. Mathematically,

$$y(x) = f(x) + Z(x) \tag{3}$$

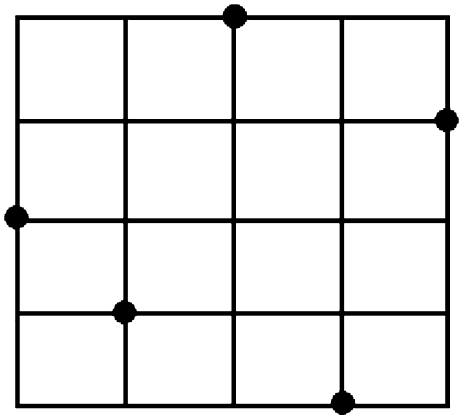

FIGURE 6. Two variables with five levels sampling using LHS scheme of DOCE.

In Eq. (3), $y(x)$ indicates the unknown function to be estimated and $f(x)$ is a polynomial-function based model designed to indicate the general trend over the design space, and $Z(x)$ represents a stochastic process with a zero mean value, variance σ^2, and non-zero covariance. The purpose of $Z(x)$ is to create a localized deviation by quantifying the interpolation values between sampling points with a correlation function, and the covariance matrix of $Z(x)$ is represented by:

$$\operatorname{cov}\left[Z\left(x^i\right), Z\left(x^j\right)\right] = \sigma^2 \boldsymbol{R}\left[R\left(x^i, x^j\right)\right], \quad i,j = 1,2,\ldots n \tag{4}$$

In Eq. (4), $\boldsymbol{R}$ stands for the correlation matrix consisting of a spatial correlation function, and $R(x^i, x^j)$ is the correlation function between any two sampling points x^i and x^j, σ^2 is the variance which depicts the scalar of the spatial correlation function quantifying the correlation between x^i and x^j, and it can control the smoothness of the Kriging model, the effect of the nearby points, and differentiability of the surface.

Generally, variations in different variables result in changes of different magnitudes in the responses. For example, if the oscillations in the response are twice as dense in one direction as opposed to others, the variogram range should be adjusted accordingly, i.e., twice as small. For anisotropic Kriging, the covariance function $\operatorname{cov}[Z(x^i), Z(x^j)]$ is computed considering different variogram ranges for each single input variable, with a common sill and nugget.[34] In this study, a popular correlation function known as the Gaussian correlation function was utilized. The Gaussian function can provide a relatively smooth and infinitely differentiable surface, so it is a preferable correlation function when a gradient-based optimization algorithm is to be adopted next stage. The regression parameter, R^2, used as an error indicator to gauge the accuracy of the anisotropic Kriging model, is represented as follows:

$$R^2 = 1 - \frac{\sum_{i=1}^{n} (y_i - \tilde{y})^2}{\sum_{i=1}^{n} (y_i - \bar{y})^2} \tag{5}$$

In Eq. (5), y_i is the actual value, $\tilde{y}$ is the value predicted by the anisotropic Kriging model, and $\bar{y}$ is the average of all actual values. When R^2 calculated from the anisotropic Kriging model is sufficiently close to one, the process of constructing the approximated model stops. Otherwise, new sampling points are added to update the approximated model.

As the first step to test the accuracy of the anisotropic Kriging model, four additional FE model simulations were performed based on random sampling. If the regression parameter R^2 was below 0.95, which indicated that the initial response surface based on the first 12 simulations was not ideal; results from all 16 simulations were used to construct a second response surface. The accuracy of the second response surface was then tested by four additional FE simulations, also based on random sampling. This procedure was continued until the resulting regression parameter R^2 was greater than 0.95, which indicated that the resulting response surface was accurate enough to identify the design parameters. This step also demonstrated that the anisotropic Kriging model approach maps the relationship between the material parameters and the assessment index F in an acceptably accurate manner.

Sequential Quadratic Programming Algorithm

A sequential quadratic programming algorithm was used as the optimization strategy to minimize the objective function in this material identification problem. This programming method is one of the most powerful nonlinear programming algorithms for solving differentiable nonlinear programming problems in an efficient and reliable way.[3,13] Many nonlinear programming problems, such as least squares or min–max optimization, can be solved using this method. Within each numerical iteration, the basic idea is to solve a quadratic programming sub-problem that is formulated by replacing the objective function with a quadratic approximation and replacing the constraint function by linear approximation. The three main steps included in the sequential quadratic programming implementation are: updating the Hessian matrix of the Lagrangian function, solving the quadratic programming sub-problem, and the formation of a new iteration using a line search.[3,13]

RESULTS AND DISCUSSION

Identical optimization procedures were applied for 20 skull samples and FE models. Through this method, each experimental force–deflection curve was matched to the simulation curve using the most favorable material parameters obtained from optimization-based material identification calculation (Figs. 7, 8). Furthermore, the optimized material parameters and assessment index F are listed in Tables 3 and 4. Different samples may have varying numbers of sampling points, response surface accuracies, and assessment index values. The numbers of LHS sampling points were all 12, and the numbers of additional sampling points ranged from 0 to 8. The quantitative accuracies of the anisotropic Kriging model (R^2) ranged from 0.966 to 0.998.

The average differences between experimental data and simulation results were 0.378 N (which was 3.3% of the force peak value) at 200 mm/s and 0.227 N (which was 2.7% of the force peak value) at 0.02 mm/s. From Fig. 7 and Table 3, it can be seen that sample 7 had the best curve fitting result with an assessment index value of 0.242 N, which is less than 2.6% of the peak force measured, while the worst fit, sample 3, was still acceptable with an assessment index value of 0.771 N, less than 5.1% of the peak force measured. Similarly, as Fig. 8 and Table 4 show, sample 6 had the best curve fitting result with the assessment index value of 0.094 N, less than 1.3% of the peak force measured, and sample 16 had the poorest curve fitting result with the assessment index value of 0.638 N, less than 5.8% of the peak force measured. The average most favorable material parameters for the 200 mm/s test group were a Young's modulus of 16.38 (±2.00) GPa, yield stress of 0.124 (±0.013) GPa, tangent modulus of 0.52 (±0.46) GPa, and failure strain of 0.067 (±0.019) as shown in Table 3. Simultaneously, for a quasi-static velocity of 0.02 mm/s, the average optimized parameters were a Young's modulus of 9.10 (±1.31) GPa, yield stress of 0.106 (±0.019) GPa, tangent modulus of 0.027 (±0.028) GPa, and failure strain of 0.085 (±0.032) as shown in Table 4.

Force–deflection curves measured from rat skull samples showed a very small nonlinearity at the very beginning in 15 out of the 20 specimens tested, similar to those depicted by Currey and Butler.[5] The maximum forces in the nonlinear region were all below 0.46 N. These slight nonlinear regions were removed by extrapolating the force–deflection curve in the linear region back to zero force. We performed such analysis for two reasons. Firstly, only the slope of initial straight line portion of the force–deflection curve was needed to calculate the Young's modulus. Therefore, the effect of the initial nonlinearity was neglected in order to compare our analysis with that obtained from traditional method. Secondly, skull samples were not perfectly flat when they were placed on top of the three-point bending fixture. As a result, only part of the specimen was loaded initially and hence the nonlinear response was mainly from stabilization of the specimen in the beginning of three-point bending tests. The potential Hertzian contact between the steel rollers and the rat skull samples should be small. Using Eq. (6) below, the calculated indentation depth due to Hertzian contact was only 3.01×10^{-5} mm with P as 0.5 N, L as 3.5 mm, E_1 as 210 GPa, v_1 as 0.30, E_2 as 5.917 GPa, and v_2 as 0.22. However, for tests within the nano range, the Hertzian contact could affect results significantly, and an unloading protocol would be needed.[27]

$$d = \frac{4P}{\pi L}\left(\frac{(1-v_1^2)}{E_1} + \frac{(1-v_2^2)}{E_2}\right) \tag{6}$$

where d is indentation depth, P is the loading force, E_1 and v_1 are the modulus and Poisson's ratio for steel, E_2 and v_2 are the modulus and Poisson's ratio for skull. L is length of the bone sample.

Based on classical beam theory (Eq. 1), the Young's modulus for the 200 mm/s group was 9.49 GPa with the standard deviation 1.86 GPa. The Young's modulus for 0.02 mm/s group was 5.92 GPa with the standard deviation 0.763 GPa. Comparing with Gefen's data (6.01 MPa) reported in 2003,[8] the values obtained from this optimization study are much larger than Gefen's results, and are in the same order of magnitude as the analytical solution based on classical beam theory. The analytical method tends to underestimate the elastic moduli because the samples are simplified as perfect beam without considering internal porosity, curvature, and change of thickness.

Mechanical properties of the rat skull may affect intracranial responses during *in vivo* TBI experiments in which the skull is either open (such as in a controlled cortical impact) or close (such as in a Marmarou weight drop). Initially, it was hoped that the effect of structural inhomogeneity could be eliminated through the use of Micro CT and specimen-specific FE models to yield a narrower range in mechanical properties. However, the optimized Young's modulus still varied greatly ranging from 14.0 to 19.5 GPa at a loading velocity of 200 mm/s and 7.1 to 10.7 GPa at a loading velocity of 0.02 mm/s. Future work should consider the inclusion of material property assignment based on gray scale values measured using Micro CT into optimization processes to better quantify the mechanical properties of rat skull so that intracranial responses can be more accurately predicted.

Human cranial bones have been reported to be transversely isotropic in directions tangent to the skull surface.[21,35] In contrast, facial bones are subjected to

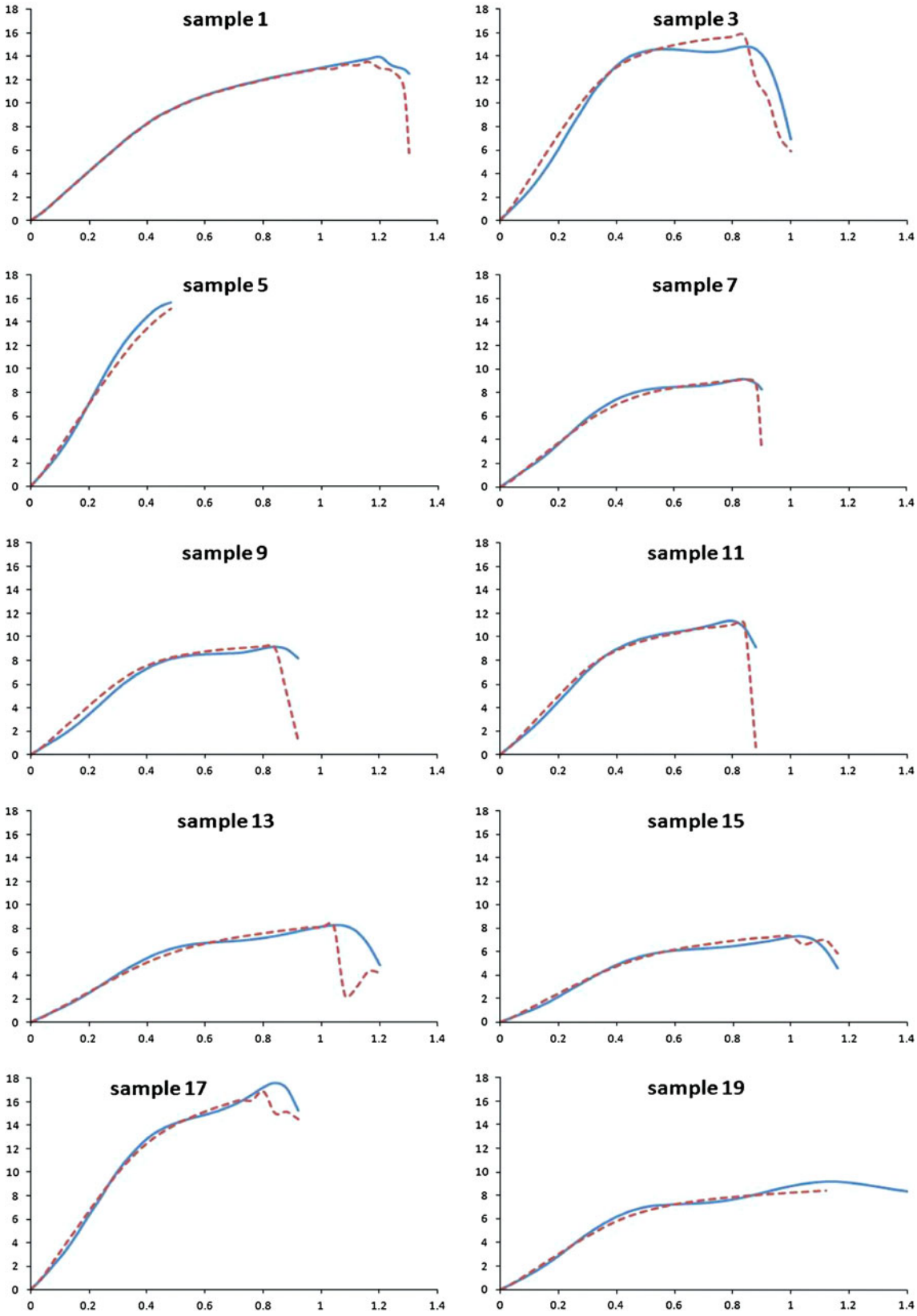

FIGURE 7. Comparison between experimental curves and simulation results (200 mm/s). *Solid lines* experimental curves, *dash lines* simulation curves. Horizontal axis unit: deflection (mm), vertical axis unit: force (N).

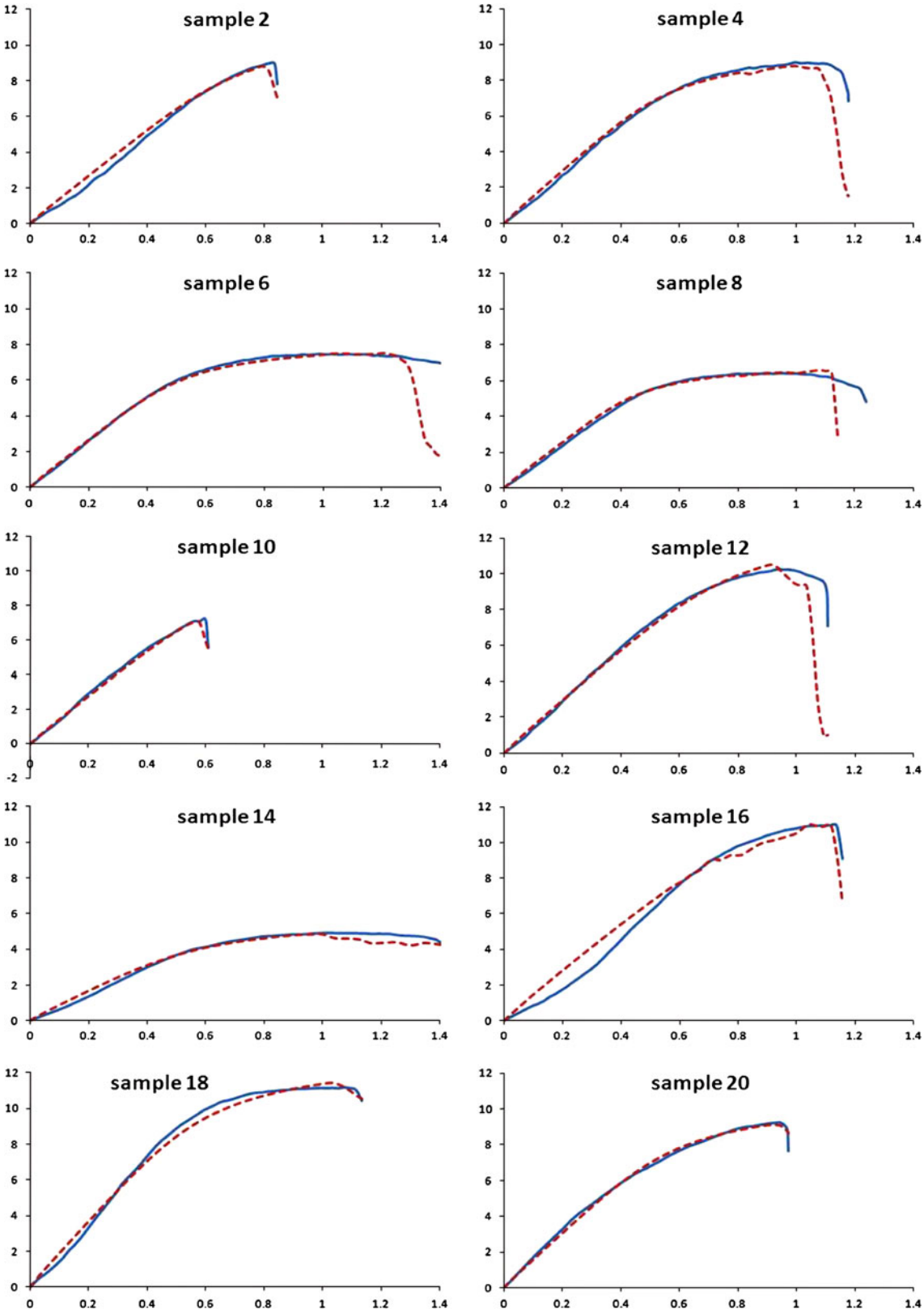

FIGURE 8. Comparison between experimental curves and simulation results (0.02 mm/s). *Solid lines* experimental curves, *dash lines* simulation curves. Horizontal axis unit: deflection (mm), vertical axis unit: force (N).

TABLE 3. Optimal material parameters for loading velocity of 200 mm/s.

Sample	*E* (GPa)	*Y* (GPa)	Et (GPa)	FS	*F* (N)
1	14.47	0.121	1.25	0.059	0.294
3	19.50	0.148	0.01	0.105	0.771
5	17.50	None	None	None	0.639
7	16.08	0.105	0.10	0.048	0.242
9	17.73	0.133	0.05	0.075	0.389
11	19.09	0.116	0.71	0.052	0.269
13	15.80	0.127	1.00	0.060	0.244
15	14.00	0.125	0.70	0.080	0.269
17	15.51	0.131	0.74	0.058	0.312
19	14.10	0.113	0.10	None	0.349
Average	16.38	0.124[a]	0.52[a]	0.067[b]	0.378
S.D.	2.00	0.013[a]	0.46[a]	0.019[b]	0.181

S.D. standard deviation, *E* Young's modulus, *Y* yield stress, *Et* tangent modulus, *FS* failure strain, *F* assessment index.
[a]Exclude sample #5.
[b]Exclude sample #5 and #19.

TABLE 4. Optimal material parameters for loading velocity of 0.02 mm/s.

Sample	*E* (GPa)	*Y* (GPa)	Et (GPa)	FS	*F* (N)
2	9.36	0.132	0.050	0.052	0.320
4	8.50	0.094	0.050	0.097	0.188
6	8.98	0.087	0.005	0.125	0.094
8	10.70	0.082	0.010	0.060	0.133
10	10.50	0.132	0.090	0.047	0.120
12	7.80	0.120	0.005	0.060	0.161
14	9.77	0.090	0.031	0.115	0.160
16	7.11	0.120	0.005	0.095	0.638
18	7.64	0.094	0.015	0.135	0.321
20	10.63	0.105	0.012	0.065	0.138
Average	9.10	0.106	0.027	0.085	0.227
S.D.	1.31	0.019	0.028	0.032	0.164

S.D. standard deviation, *E* Young's modulus, *Y* yield stress, *Et* tangent modulus, *FS* failure strain, *F* assessment index.

masticatory loads and may exhibit directionally dependent material properties. Studies on an FE human mandible model demonstrated that the FE-predicted peak volumetric strain decreased when considering anisotropic elasticity.[11,15] These anisotropic characteristics were also confirmed through microindentation experiments by Daegling *et al.*[6] In the only published study to investigate rat skull material properties experimentally, Gefen *et al.*[8] analyzed the tissue as an isotropic elastic material. Therefore, for the current study, isotropic elastic–plastic behavior was assumed based on human data published by McElhaney *et al.*[21] and Wood,[35] as well as the rat data from the Gefen *et al.*[8] study. This is believed to be appropriate because the rat skull is thin and shell-like, which makes it very difficult to study material behavior in the axis perpendicular to the skull surface and to date no rat skull properties have been reported for this direction in the literature. In future studies, the potential anisotropic property of rat skull could be studied experimentally along three mutually perpendicular axes, CT imaging with elastic trajectories,[11] and FE simulations with elasticity tensors defined accordingly.

The proposed optimization-based material identification methodology is a helpful tool to efficiently and accurately reveal material parameters through reverse engineering, providing scientific basis for FE model development. Considering that each skull sample was naturally curved, different thickness and varying porosities as shown from micro CT images, specimen-specific FE models served to eliminate such geometric effect. While in the conventional beam theory, the skull sample was ideally assumed as perfect rectangular, flat, with uniform thickness, and without porosity. Such simplification and idealization when applying classical beam theory could induce errors in calculating material parameters.

CONCLUSIONS

This paper proposed an application of optimization methodology to biomaterial parameter identification through the combination of the sample-specific FE models, anisotropic Kriging modeling, and sequential quadratic programming. The anisotropic Kriging model predicted results show excellent accuracy to the experiments. Using anisotropic Kriging to construct the response surface model and optimize the objective function through sequential quadratic programming, the relationships among the material parameters and force–deflection curves can be mapped accurately, reducing the total simulation time and improving accuracy of the material parameters. The method was applied to a typical rat skull material identification problem. Through this study, the rat skull material property parameters (such as the Young's modulus, yield stress, tangent modulus, and failure strain as described in Tables 3 and 4) were obtained for two different loading speeds. The same method can be adapted to other reversing engineering procedures to obtain accurate material parameters for FE models development.

ACKNOWLEDGMENTS

This study is supported by the National 973 Program under Grant number 2010CB832705 and the National Science Fund for Distinguished Young Scholars (10725208), both funded through the Chinese government. The primary author of this manuscript is supported by a fellowship provided by the China Scholarship Council funded by the Ministry of Education of the People's Republic of China and in part by the Bioengineering Center at Wayne State University.

REFERENCES

[1]Barber, T. W. Static compression testing of specimens from an embalmed human skull. *Tex. Rep. Biol. Med.* 28(4):497–508, 1970.

[2]Bates, R. A., R. J. Buck, E. Riccomagno, and H. P. Wynn. Experimental design and observation for large systems. *J. R. Stat. Soc. B* 58:77–94, 1996.

[3]Boggs, P. T., and J. W. Tolle. Sequential quadratic programming for large-scale nonlinear optimization. *J. Comput. Appl. Math.* 124:123–137, 2000.

[4]Chawla, A., S. Mukherjee, and B. Karthikeyan. Characterization of human passive muscles for impact loads using genetic algorithm and inverse finite element methods. *Biomech. Model. Mechanobiol.* 8:67–76, 2009.

[5]Currey, J. D., and G. Butler. The mechanical properties of bone tissue in children. *J. Bone Joint Surg.* 57:810–814, 1975.

[6]Daegling, D. J., J. L. Hotzman, W. S. McGraw, and A. J. Rapoff. Material property variation of mandibular symphyseal bone in colobine monkeys. *J. Morphol.* 270:194–204, 2009.

[7]Fang, K.-T., R. Li, and A. Sudjianto. Design and modeling for computer experiments. Boca Raton: Taylor & Francis Group, 2006.

[8]Gefen, A., N. Gefen, Q. Zhu, R. Raghupathi, and S. S. Margulies. Age-dependent changes in material properties of the brain and braincase of the rat. *J. Neurotrauma* 20:1163–1177, 2003.

[9]Gu, L., and R. J. Yang. Recent applications on reliability-based optimization of automotive structures. SAE Technical Paper Series, 2003-01-0152, 2003.

[10]Hallquist, J. O. LS-DYNA Theoretical Manual. Livermore, CA: Livermore Software Technology Co, 2005.

[11]Hellmich, C., C. Kober, and B. Erdmann. Micromechanics-based conversion of CT data into anisotropic elasticity tensors, applied to FE simulations of a mandible. *Ann. Biomed. Eng.* 36(1):108–122, 2008.

[12]Jourdan, A. How to repair a second-order surface for computer experiments by Kriging. *Chemom. Intell. Lab. Syst.* 96(2):108–116, 2009.

[13]Kim, K.-Y., and D.-Y. Shin. Optimization of a staggered dimpled surface in a cooling channel using Kriging model. *Int. J. Therm. Sci.* 47(11):1464–1472, 2008.

[14]Kim, J. E., Z. P. Li, Y. Ito, C. D. Huber, A. M. Shih, A. W. Eberhardt, K. H. Yang, A. I. King, and B. K. Soni. Finite element model development of a child pelvis with optimization-based material identification. *J. Biomech.* 42:2191–2195, 2009.

[15]Kober, C., B. Erdmann, C. Hellmich, R. Sader, and H. F. Zeilhofer. Consideration of anisotropic elasticity minimizes volumetric rather than shear deformation in human mandible. *Comput. Methods Biomech. Biomed. Eng.* 9(2):91–101, 2006.

[16]Koehler, J. R., and A. B. Owen. Computer experiments. In: Handbook of Statistics, 13: Designs and Analysis of Experiments, edited by S. Ghosh, and C.R. Rao. North-Holland: Amsterdam, 1996, pp. 261–308.

[17]Levchakov, A., E. Linder-Ganz, R. Raghupathi, S. S. Margulies, and A. Gefen. Computational studies of strain exposures in neonate and mature rat brains during closed head impact. *J. Neurotrauma* 23:1570–1580, 2006.

[18]Mao, H., X. Jin, L. Zhang, K. H. Yang, T. Igarashi, L. Noble-Haeusslein, and A. I. King. Finite element analysis of controlled cortical impact induced cell loss. *J. Neurotrauma* 27:877–888, 2010.

[19]Mao, H., K. H. Yang, A. I. King, and K. Yang. Computational neurotrauma—design, simulation, and analysis of controlled cortical impact model. *Biomech. Model. Mechanobiol.*, 2010. doi:10.1007/s10237-010-0212-z.

[20]Mao, H., L. Zhang, K. H. Yang, and A. I. King. Application of a finite element model of the brain to study traumatic brain injury mechanisms in the rat. *Stapp Car Crash J.* 50:583–600, 2006.

[21]McElhaney, J. H., J. L. Fogle, J. W. Melvin, R. R. Haynes, V. L. Roberts, and N. M. Alem. Mechanical properties on cranial bone. *J. Biomech.* 3:495–511, 1970.

[22]McKay, M. D., R. J. Beckman, and W. J. Conover. A comparison of three methods for selecting values of input variables in the analysis of output from a computer code (JSTOR Abstract). *Technometrics* 21(2):239–245, 1979.

[23]Melvin, J. W., D. H. Robbins, and V. L. Roberts. The mechanical properties of the diploë layer in the human skull in compression. Developments in Mechanics 5:811–818, 1969. Paper No. 05-0250.

[24]Pena, A., J. D. Pickard, D. Stiller, N. G. Harris, and M. U. Schuhmann. Brain tissue biomechanics in cortical contusion injury: a finite element analysis. *Acta Neurochir. Suppl.* 95:333–336, 2005.

[25]Rasmussen, C. E., and C. K. I. Williams. Gaussian Processes for Machine Learning. Cambridge: MIT Press, 2006.

[26]Reimann, D. A., S. M. Hames, M. J. Flynn, and D. P. Fyhrie. A cone beam computed tomography system for true 3d imaging of specimens. *Appl. Radiat. Isot.* 48(10–12): 1433–1436, 1997.

[27]Rho, J. Y., J. D. Currey, P. Zioupos, and G. M. Pharr. The anisotropic Young's modulus of equine secondary osteones and interstitial bone determined by nanoindentation. *J. Exp. Biol.* 204:1775–1781, 2001.

[28]Robbins, D. H., and J. L. Wood. Determination of mechanical properties of the bones of the skull. *Exp. Mech.* 9(5):236–240, 1969.

[29]Sacks, J., S. B. Schiller, and W. J. Welch. Designs for computer experiments. *Technometrics* 31:41–47, 1989.

[30]Sacks, J., W. J. Welch, T. J. Mitchell, and H. P. Wynn. Design and analysis of computer experiments. *Stat. Sci.* 4(4):409–423, 1989.

[31]Santner, T. J., B. J. Williams, and W. Notz. The design and analysis of computer experiments. New York: Springer Series in Statistics, Springer, 2003.

[32]Untaroiu, C., K. Darvish, J. Crandall, B. Deng, and J. T. Wang. Characterization of the lower limb soft tissues in pedestrian finite element models. *The 19th International Technical Conference on the Enhanced Safety of Vehicles*. US Department of Transportation, National Highway Traffic Safety Administration, Washington, DC, 2005.

[33]Untaroiu, C., J. Kerrigan, and J. Crandall. Material identification using successive response surface methodology, with application to a human femur subjected to three-point bending loading, SAE Technical Paper Number 2006-01-0063. Warrendale, PA, 2006.

[34]Wackernagel, H. Multivariate Geostatistics: An Introduction with Applications. New York: Springer, 2003.

[35]Wood, J. L. Dynamic response of human cranial bone. *J. Biomech.* 4:1–12, 1971.

[36]Zhang J. A finite element modeling of anterior lumbar spinal fusion, M.S. Thesis, Wayne State University, 1992.